Stability Analysis of Damping Control to Suppress Filter Resonance in Multi-modular Matrix Converter

Hiroki Takahashi
Dept. of Energy and Environmental Science
Nagaoka University of Technology
Nagaoka Niigata, Japan
thiroki@stn.nagaokaut.ac.jp

Jun-ichi Itoh
Dept. of Energy and Environmental Science
Nagaoka University of Technology
Nagaoka Niigata, Japan
itoh@vos.nagaokaut.ac.jp

Abstract— **This paper discusses a stability analysis for a damping control to suppress the LC filter resonance in a multi-modular matrix converter. The damping control is combined with the output current control of the system to reduce the current distortion which is caused by the LC resonance. The stability is analyzed by using the Bode-diagrams of an integrated block diagram of the multi-modular matrix converter. In the simulation, the damping control ensures the gain margin of 4.5 dB, and the system obtains stability. Moreover, from the experimental result, the stable operation of the multi-modular matrix converter is confirmed and the primary current THD of the transformer is 5.0 %. In addition, the transient response characteristics are evaluated, which is based on the overshoot value of the output current with respect to the gain margin in experiments.**

I. INTRODUCTION

Medium voltage applications such as the wind turbines have received significant focus recently. In order to achieve high efficiency and light weight of the system, the multi-modular matrix converter which is a matrix converter topology for medium voltage applications is investigated [1]-[4]. The multi-modular matrix converter consists of a multiple winding transformer and several modules of a three-phase to single-phase matrix converter with small filter capacitors. Therefore, the multi-modular matrix converter promises to achieve higher efficiency, smaller size and longer life-time compared to the multi-modular voltage source converter-inverter system.

However, it has been found that the multi-modular matrix converter has a LC resonance problem which is caused by the leakage inductances of the transformer and the capacitors in the input filters of the modules. This filter resonance leads to deteriorate the input current quality, and cannot be suppressed by damping resistors practically.

In order to overcome this resonance problem in the multi-modular matrix converter, a damping control combined with the output current control, which the output current control (a part of a field oriented control) is required for an adjustable speed drive system of a motor, has been discussed and its validity has been confirmed [5]. The damping control combined with the output current control is more cost-effective compared with the conventional damping controls which require voltage sensors at the input stage [6]-[8].

Previous studies regarding the conventional damping controls for general matrix converters describe the design equation for the control parameters [6]-[7]. However, the design equation cannot be expanded into the proposed damping control. In contrast, a damping control combined with the output current control for a general matrix converter topology has been discussed [9]. This control strategy achieves the resonance suppression and also is able to control the output current at the same time. However, in the multi-modular matrix converter, the stability and transient response of not only a module but the whole system is important and therefore this paper discusses the design method of the damping control parameters which is subject to the damping effect and the transient response of the output current.

In this paper, a stability analysis method of the multi-modular matrix converter including the damping control is described. The proposed analysis method uses Bode-diagram based on the integrated block diagram of the whole system which is composed of the circuit and the control block diagram. Thus, the damping control and the output current control can be designed easily since the effects of the resonant suppression and the output current response are yielded from the Bode-diagrams. Firstly, the system block diagram of the multi-modular matrix converter with the damping control and the output current control are described. Secondly, an integrated block model of the multi-modular matrix converter is derived based on the concept of duty-cycle space vector [10]. Thirdly, the stability of the multi-modular matrix converter is analyzed with the Bode-diagrams. Finally, the validity of the proposed stability analysis is confirmed in simulation and experimental results.

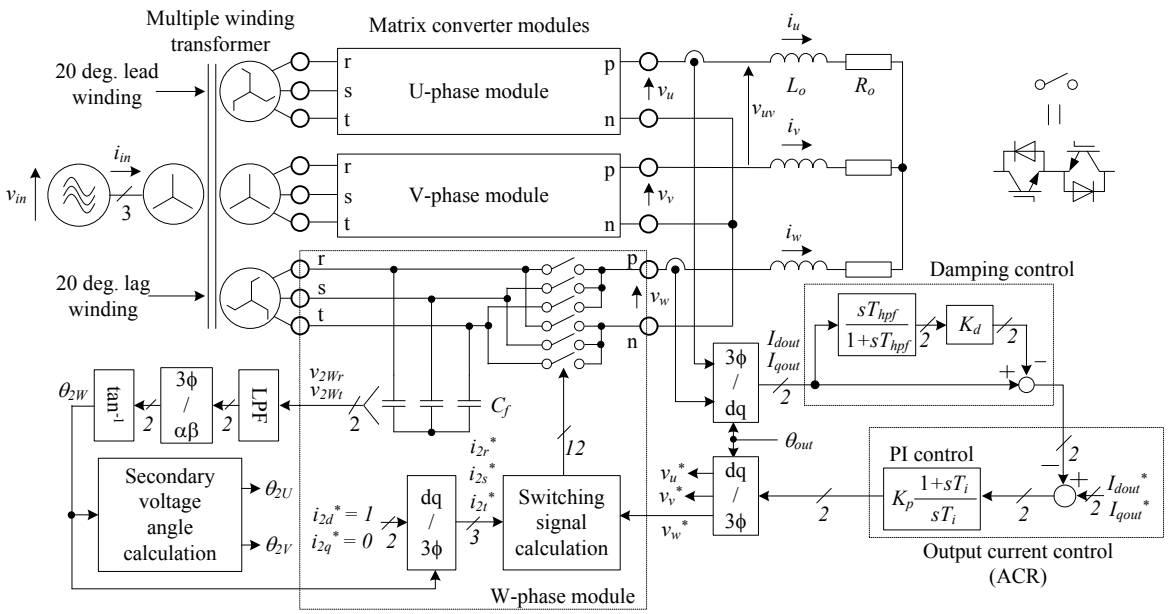

Figure 1. System diagram of a multi-modular matrix converter employing three modules with the damping control. Note that the configuration of U, V-phase modules is the same as W-phase. The output voltage control block includes the damping control and an ACR.

II. Multi-modular Matrix Converter Employing Damping Control Combined with Output Stage

Fig. 1 shows the system diagram of a three modules multi-modular matrix converter This paper only considers a three-module model due to the simplicity, which in practical a nine modules multi-modular matrix converter is required for a medium voltage application [1]-[4]. For the same reason, a constant power load composed by an R-L load and an ACR (auto current regulator) for the output current is used, not a motor controlled by a field oriented control. A multiple winding transformer is located between the power source and matrix converter modules. The transformer cancels the low order harmonics in the primary current of the transformer and reduces the ripples in the output voltage due to phase shift of the secondary windings by 20 degrees. Each matrix converter module consists of a three-phase to single-phase matrix converter which controls output phase voltage and secondary current of the transformer, and the small filter capacitors.

As mentioned previously, the multi-modular matrix converter has the LC resonance problem due to leakage inductances of the transformer and the capacitors in the input filter of the modules. In order to suppress the distortion, a damping control combined with the output current control, which has a damping gain K_d and a damping HPF (high pass filter) with a time constant T_{hpf}, has been proposed [5]. The damping control is applied to the feedback path of the ACR as illustrated in Fig. 1.

The filter resonance is separated into the series resonance due to harmonics in the power source voltage and the parallel resonance triggered by a dynamic characteristic of the multi-modular matrix converter. A solution for the series resonance is to redesign the filter parameters, which changes the resonant frequency to avoid the frequency of the voltage source harmonics. However, it is difficult to suppress the parallel resonance with the redesign only. The parallel resonance is excited by the output current control with high natural frequency [11]. Therefore, the parallel resonance can be referred as the destabilization of the output current control. In order to stabilize the multi-modular matrix converter, this paper reveals Bode-diagrams derived from an integrated block diagram which is composed of the circuit and the control diagram, and the damping control is designed based on the desired gain margin. However, as shown in Fig. 1, the damping control interferes with the response of the output current control. Thus, it is necessary to evaluate the transient response of the output current with respect to the designed stability.

III. Analysis Model

A. Derivation of the Analysis Model

In order to derive the analysis model of the multi-modular matrix converter, the output voltage equation and the input current equation are required. The output voltage and the input current equations of a general three-phase to three-phase matrix converter based on the duty-cycle space vector have been presented [10]. However, these equations cannot be applied to the multi-modular matrix converter directly because the multi-modular matrix converter employs three-phase to single-phase matrix converter module. Therefore, an equivalent three-phase to three-phase matrix converter model which provides the same output voltage and the input current as the multi-modular matrix converter is considered.

Fig. 2 shows the equivalent model based on a three-phase to three-phase matrix converter corresponding to the multi-modular matrix converter. This equivalent model has a three-

phase LC filter, a three-phase transformer and a three-phase to three-phase matrix converter. The filter inductor L_{fp} corresponds to the leakage inductance of the multiple winding transformer in Fig. 1. In contrast, the filter capacitor is converted to the primary side of the three-phase transformer and the equivalent capacitance C_{fp} is presented by (1).

$$C_{fp} = n\left(\frac{V_2}{V_1}\right)^2 C_f \tag{1}$$

where, n is the number of the modules and V_2/V_1 is the voltage transformation ratio of the multiple winding transformer in Fig. 1. The three-phase transformer in Fig. 2 is adopted to obtain the same output voltage as the multi-modular matrix converter. Then, the output voltage amplitude of the multi-modular matrix converter V_{out_mmmc} is expressed by (2).

$$V_{out\_mmmc} = \frac{mn}{2}\left(\frac{V_2}{V_1}\right)V_{in} \tag{2}$$

where, m is the modulation index and V_{in} is the amplitude of the source voltage. In contrast, the output voltage amplitude of the equivalent model V_{out_emc} is presented by (3).

$$V_{out\_emc} = \frac{\sqrt{3}}{2} maV_{in} \tag{3}$$

where, a is a turn ratio of the three-phase transformer in Fig. 2. In order that the equivalent model yields the same output voltage as the multi-modular matrix converter, a is defined as following.

$$a = \frac{n}{\sqrt{3}}\left(\frac{V_2}{V_1}\right) \tag{4}$$

Therefore, the analysis block model is obtained by using the equivalent model in Fig. 2 and the concept of the duty-cycle space vector.

Fig. 3 shows the integrated block model of the equivalent matrix converter circuit and the control diagram. Variables in the bold font represent their space vectors. For example, the input voltage vector $\boldsymbol{v_{in}}$ is defined as following.

$$\boldsymbol{v_{in}} = \frac{2}{3}\left(v_r + v_s e^{j\frac{2}{3}\pi} + v_t e^{-j\frac{2}{3}\pi}\right) \tag{5}$$

where, v_r is the input R-phase voltage, v_s is the input S-phase voltage and v_t is the input T-phase voltage.

In order to connect the input and output circuits of the equivalent model, the duty-cycle space vector $\boldsymbol{m_d}$ and $\boldsymbol{m_i}$ are introduced and the output voltage vector $\boldsymbol{v_{out}}$ is yielded by (6).

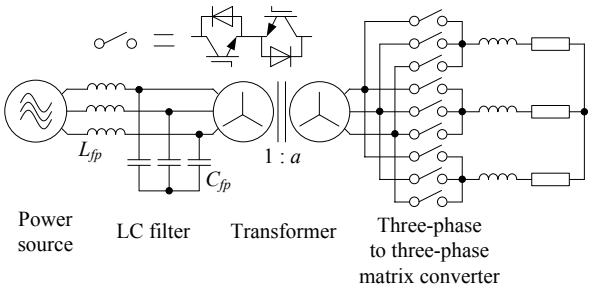

Figure 2. Equivalent three-phase to three-phase matrix converter model corresponding to the multi-modular matrix converter in Fig. 1.

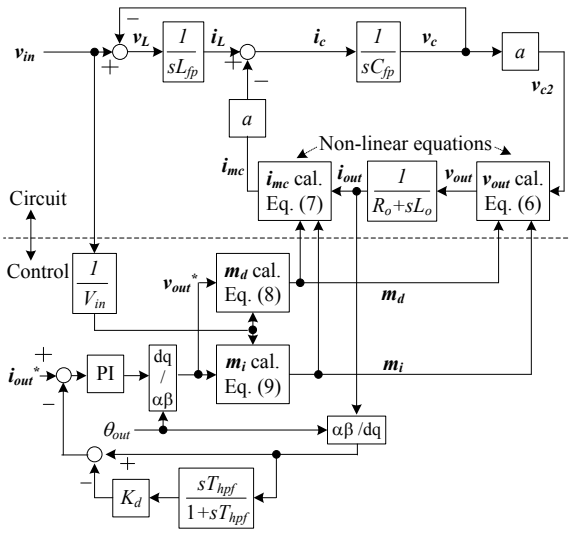

Figure 3. Integrated block model of the equivalent matrix converter which is composed of the circuit and the control diagram. This block diagram is based on the duty-cycle space vector.

$$\boldsymbol{v_{out}} = \frac{3}{2}\overline{\boldsymbol{m_i}}\boldsymbol{v_{c2}} + \frac{3}{2}\boldsymbol{m_d}\overline{\boldsymbol{v_{c2}}} \tag{6}$$

where, $\boldsymbol{v_{c2}}$ is the filter capacitor voltage converted to the secondary side of the transformer. Note that a bar placed over a variable indicates complex conjugate. On the other hand, the input current of the equivalent matrix converter $\boldsymbol{i_{mc}}$ is expressed by (7).

$$\boldsymbol{i_{mc}} = \frac{3}{2}\boldsymbol{m_i}\boldsymbol{i_{out}} + \frac{3}{2}\boldsymbol{m_d}\overline{\boldsymbol{i_{out}}} \tag{7}$$

where, $\boldsymbol{i_{out}}$ is the output current vector. Hence, the input and output circuits of the equivalent model are connected by (6) and (7). In contrast, when the input power factor reference of the multi-modular matrix converter is unity and the filter inductor voltage in steady state is much smaller than the input voltage, $\boldsymbol{m_d}$ and $\boldsymbol{m_i}$ are represented by follows.

$$\boldsymbol{m_d} = \frac{\boldsymbol{v_{in}}}{3V_i}\boldsymbol{v_{out}}^* \tag{8}$$

$$\boldsymbol{m}_i = \frac{\boldsymbol{v}_{in}}{3V_i}\overline{\boldsymbol{v}_{out}^{\,*}} \tag{9}$$

where, $\boldsymbol{v}_{out}^{\,*}$ is the output voltage reference. Therefore, the integrated block model is derived by using (6) to (9) because $\boldsymbol{v}_{out}^{\,*}$ is also the output of the control block diagram.

However, Fig. 3 has a problem, which the transient responses of $\boldsymbol{v}_{out}$ and $\boldsymbol{i}_{mc}$ indicate non-linear characteristics because the time constants of fluctuation of $\boldsymbol{v}_{c2}$, $\boldsymbol{m}_d$, $\boldsymbol{m}_i$ and $\boldsymbol{i}_{out}$ are close to each other. Therefore, a linear approximation method around the operating point at a steady state is applied to these non-linear parts. The output voltage vector $\boldsymbol{v}_{out}$ is separated into the steady and differential components, where the differential component is expressed as (10).

$$\Delta\boldsymbol{v}_{out} = \frac{3}{2}\left(\overline{\Delta\boldsymbol{m}_i\boldsymbol{v}_{c2s}} + \overline{\boldsymbol{m}_{is}\Delta\boldsymbol{v}_{c2}}\right) + \frac{3}{2}\left(\Delta\boldsymbol{m}_d\,\overline{\boldsymbol{v}_{c2s}} + \boldsymbol{m}_{ds}\,\overline{\Delta\boldsymbol{v}_{c2}}\right) \tag{10}$$

where, suffix "*s*" represents steady component based on its fundamental frequency whereas "Δ" means differential component in a transient state. In a similar way, the differential component of $\boldsymbol{i}_{mc}$ is expressed as (11).

$$\Delta\boldsymbol{i}_{mc} = \frac{3}{2}\left(\Delta\boldsymbol{m}_i\boldsymbol{i}_{outs} + \boldsymbol{m}_{is}\Delta\boldsymbol{i}_{out}\right) + \frac{3}{2}\left(\Delta\boldsymbol{m}_d\,\overline{\boldsymbol{i}_{outs}} + \boldsymbol{m}_{ds}\,\overline{\Delta\boldsymbol{i}_{out}}\right) \tag{11}$$

Fig. 4 shows the linearized block model of the equivalent matrix converter regarding the differential components. The products of space vectors which become non-linear equations as shown (6) and (7) are linearized by using sum of products of the steady vector and the differential vector. Thus, the stability and the transient characteristics of the multi-modular matrix converter are obtained by using Bode-diagram derived from Fig. 4. Note that the analysis should be implemented with DC mode in which the input and output angles are fixed because the rotating frequency of the steady vector does not equal to the rotating frequency of the differential vector.

B. Verification of the linearized model with simulation

Table 1 and Table 2 present the simulation conditions of the circuit model as illustrated in Fig. 1 and the linearized model as shown in Fig. 4. This section shows the result without the ACR and the damping control in order to evaluate the verification of the linearized model. The results with the ACR and the damping control are described in next chapter. Note that the inductor and capacitor parameters are normalized based on 50 Hz.

Fig. 5 shows the indicial response of the circuit model and the linearized model with an open-loop control in a simulation. It should be noticed that all waveforms are applied with a 1 kHz cut-off frequency LPF (low pass filter) in order to observe these average waveform without switching ripples. From Fig. 5, it is confirmed that the linearized model waveforms correspond to the circuit model result. Furthermore, the error between the circuit model and

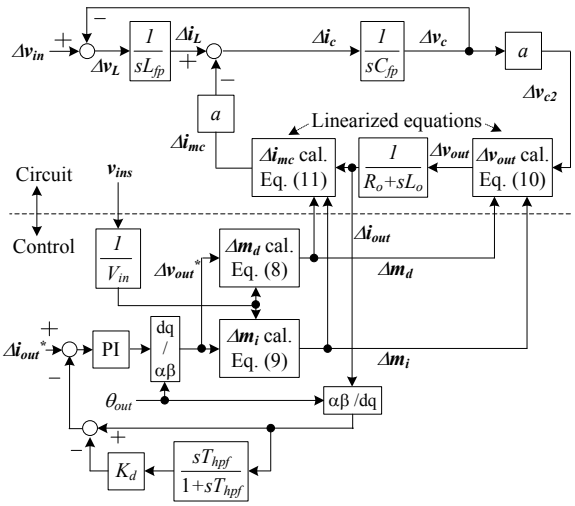

Figure 4. Linearized block model of the equivalent matrix converter regarding the differential components. The stability of the multi-modular matrix converter is obtained by analyzing this block model.

TABLE I. CIRCUIT PARAMETERS OF THE MULTI-MODULAR MATRIX CONVERTER.

Input line voltage	200 V_{rms}	Rated output voltage	300 V_{rms}
Rated power	3 kW	Carrier frequency	100 kHz
Input filter L (L_{fp})	6.65 mH (15.7%)	Load resistance (R_o)	25.2 Ω (84.0%)
Input filter C (C_f)	6.7 μF (8.42%)	Load inductance (L_o)	5.5 mH (5.76%)
Input voltage angle	105 deg.	Output voltage angle	5 deg.

TABLE II. CONTROL PARAMETERS FOR OPEN-LOOP CONTROL.

Open-loop control	d-axis voltage command (steady state)	0.5 p.u.
	d-axis voltage command (step input)	0.01 p.u.
	q-axis voltage command	0 p.u.

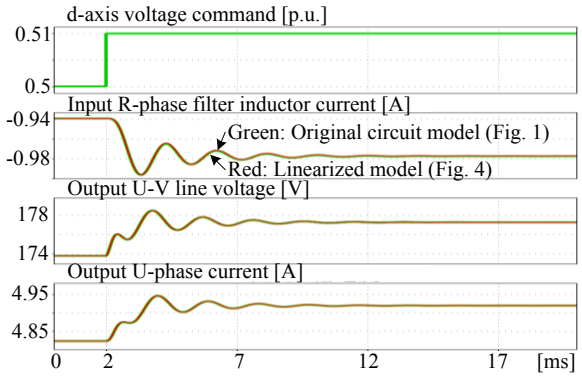

Figure 5. Indicial response of the circuit model and the linearized model with an open-loop control in a simulation. It is confirmed that the linearized model result corresponds to the circuit model result.

the linearized model waveforms is lesser than 1% in steady state. The input S-phase and T-phase waveforms, and the output V-phase and W-phase waveforms are in the same manner. Thus, the linearized model is valid for modeling of the multi-modular matrix converter.

IV. Stability Analysis using Simulation

A. Mechanism of Destabilization

Table 3 shows the parameters of the output current control of the linearized model. This section explains the mechanism of the destabilization due to the output current control and the LC filter. Thus, the damping control is not applied to the linearized model. In addition, the output current control is designed to yield the natural frequency of 650 Hz without taking the LC filter into account.

Fig. 6 shows the indicial responses of the linearized model with the designed output current control in a simulation. This simulation adds a small step of 0.01 p.u. to the output current reference at 2 ms. Fig. 6 verifies that the filter resonance is excited immediately after the step input of the output current reference, and the filter inductor current and the filter capacitor voltage contain the resonant oscillation. Moreover, the output current diverges from its command due to the resonance. Then, the oscillation frequency of the output current is 352 Hz. Therefore, in order to evince the mechanism of this destabilization, the analysis of the open-loop transfer function of the output current control is needed.

Fig. 7 shows a Bode-diagram of the open-loop transfer function of the output current control in the linearized block model without the damping control. Fig. 7 indicates the instability due to the LC filter. Fig. 7(a) shows the gain characteristics and (b) shows the phase characteristics. From Fig. 7, the gain curve without the LC filter decreases uniformly, which the ratio is -20 dB/dec. In addition, the phase curve is constant at -90 deg.. However, the gain curve taking the LC filter into account has a resonance point at 535 Hz. Then, the designed gain-crossover frequency is shifted from 650 Hz to 874 Hz and the phase is lagged drastically by the LC filter characteristic. As a result, the phase margin and the gain margin of the linearized model are obtained by -234 deg. and -4.56 dB, respectively. In this way, the multi-modular matrix converter can be unstable due to the LC resonance.

B. Parameter Design of Damping Control

Table 4 shows the damping control parameters. This section mentions the design method of the damping control.

Fig. 8 shows a Bode-diagram of the open-loop transfer function of the output current control in the linearized model as shown in Fig. 4. The transfer function of the damping control $H_{damp}(s)$ is presented as following.

$$H_{damp}(s) = \frac{1 + sT_{hpf}(1 - K_d)}{1 + sT_{hpf}} = \frac{1 + sT_2}{1 + sT_1} \qquad (12)$$

TABLE III. Parameters for Output Current Control.

Output current control (ACR)	d-axis current command (steady state)	0.75 p.u.
	d-axis current command (step input)	0.01 p.u.
	q-axis current command	0 p.u.
	ACR natural frequency	650 Hz

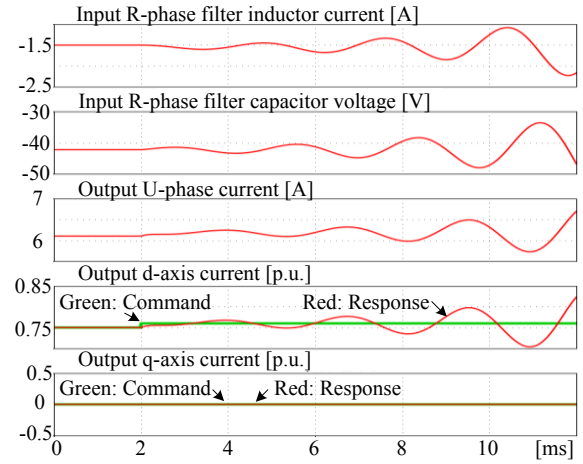

Figure 6. Indicial response of the linearized model with the output current control only in a simulation. This result shows that the filter resonance is excited and the system becomes unstable.

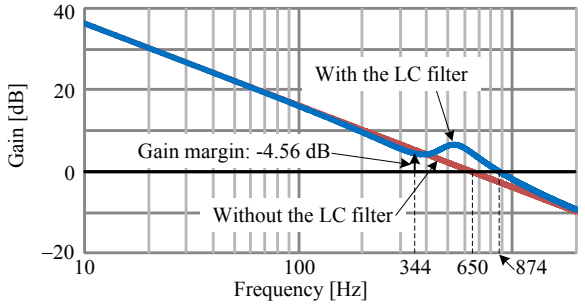

(a) Gain characteristic.

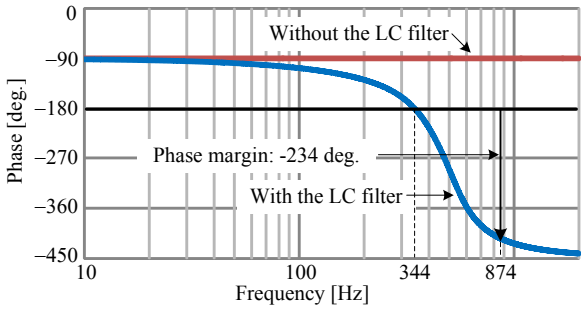

(b) Phase characteristic.

Figure 7. Bode-diagram of the open-loop transfer function of the output current control in the linearized block model without the damping control. The LC filter resonance makes the system unstable.

From (12), the damping control is equivalent to a phase lag compensator because T_2 is smaller than T_1. Hence, in order to ensure the desired gain margin g_m, the gain at the phase-crossover frequency should be decreased by the designed damping control. Note that the damping control parameters are designed based on a gain margin not a phase margin because the design based on a phase margin cannot stabilize the system for some conditions. First, the phase-crossover frequency f_{cp} is obtained from the phase curve without the damping control. Next, the gain g_a at f_{cp} is measured from the gain curve without the damping control and the damping gain K_d is calculated by the following equation.

$$\left(g_a + g_m\right) + 20\log_{10}\left(1 - K_d\right) = 0 \tag{13}$$

where, $0 < K_d < 1$, $g_a > 0$, $g_m > 0$. In contrast, in order to ensure g_m, a phase lag at f_{cp} should be zero even if the damping control is applied. Thus, a time constant of the HPF of the damping control T_{hpf} is designed by using (14), which is based on a break point approximation of a Bode-diagram.

$$T_{hpf} = \frac{5}{2\pi\left(1 - K_d\right) f_{cp}} \tag{14}$$

The gain and the phase curves with the damping control in Fig. 8 are the result when the damping control is designed in order to obtain the gain margin of 5 dB. Note that the designed K_d and T_{hpf} are shown in Table 4. From Fig. 8, the designed damping control decreases the gain at f_{cp} and yields the actual gain margin of 4.5 dB. As a result, the system achieves a stable operation. The error between the desired and the actual gain margins is caused by the break point approximation of a Bode-diagram of (14).

Fig. 9 shows the indicial response of the linearized model with the output current control and the designed damping control in a simulation. The resonant oscillation in the output current is suppressed by the damping control. As a result, all waveforms converge toward their steady points. Therefore, the proposed damping control achieves the resonant suppression and the output current control at the same time. However, the overshoot of the output current response is obtained by 261% and the cause of this overshoot is the damping control.

C. Transient Response of Output Current Control

Fig. 10 shows a Bode-diagram of the closed-loop transfer function of the output current control in the linearized block model in order to evaluate the overshoot of the output current in a transient response. When the damping control is not introduced, the gain curve is less than 3 dB under 250 Hz and has a resonance point at 352 Hz. On the other hand, the damping control increases the gain curve in the lower frequency bandwidth and generates larger overshoot of the output current than the designed value. In addition, the gain in the lower frequency bandwidth increases with respect to the designed gain margin. Thus, a tradeoff relationship

TABLE IV. PARAMETERS FOR DAMPING CONTROL.

Damping control	Damping gain (K_d)	0.67 p.u.
	Damping HPF time constant (T_{hpf})	7.0 ms

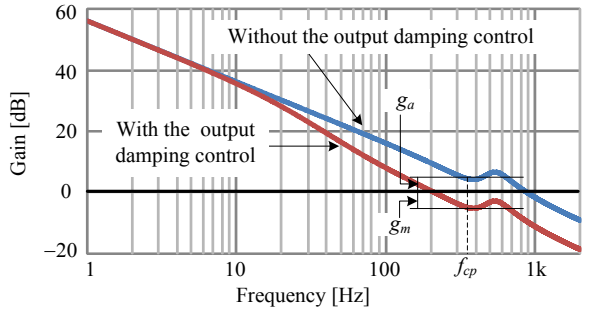

(a) Gain characteristic.

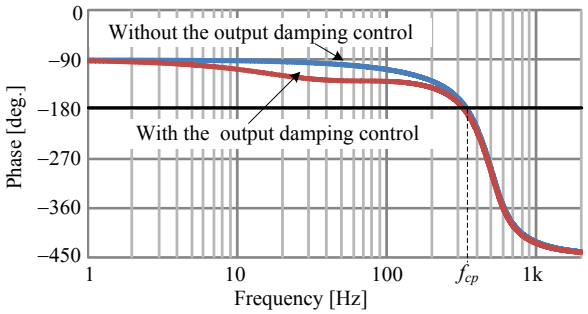

(b) Phase characteristic.

Figure 8. Bode-diagram of the open-loop transfer function of the output current control in the linearized block model in Fig. 4. f_{cp} is the phase-crossover frequency, and g_m is the desired gain margin. The damping control makes the system stable with the gain margin of 4.5 dB.

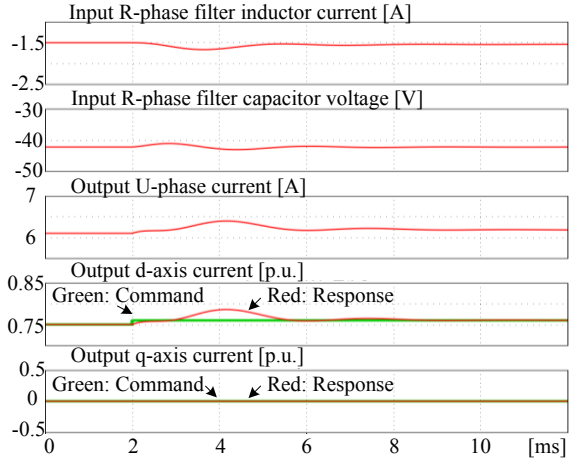

Figure 9. Indicial response of the linearized model with the output current control and the damping control in a simulation. This result shows that the damping control stabilize the system. However, the damping control generates the overshoot of the d-axis current of 261%.

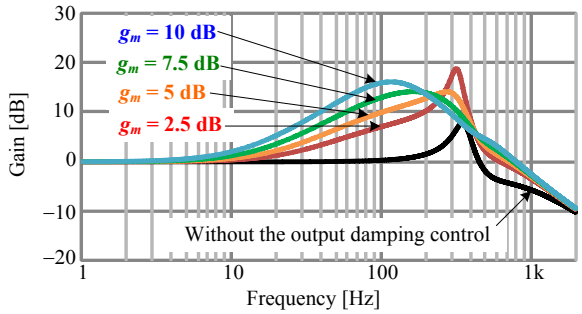

(a) Gain characteristic.

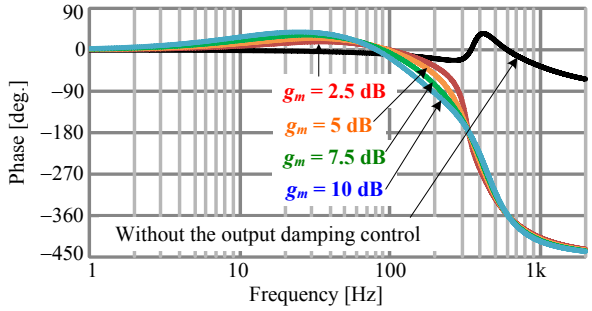

(b) Phase characteristic.

Figure 10. Bode-diagram of the closed-loop transfer function of the output current control in the linearized block model as drawn in Fig. 4. g_m is the desired gain margin. The damping control increases the gain in the lower frequency bandwidth and generates larger overshoot of the output current than the designed value.

between the stability and the transient response is demonstrated.

V. Experimental Results

This chapter evaluates the damping effect and the transient response of the multi-modular matrix converter prototype with the designed damping control as shown in Fig.1. The prototype parameters are almost consistent with the parameters shown from Table 1 to Table 4. However, the input voltage is 50 Hz while the output voltage is 30 Hz. In addition, the output d-axis current reference is separated into the steady component of 0.75 p.u. and the step component of 0.05 p.u.. Furthermore, the carrier frequency is set to 10 kHz. The modulation of the matrix converter module employs the method as introduced in [12].

Fig. 11 shows the input and output waveforms of the multi-modular matrix converter obtained by the experiments. Fig. 11 (a) shows the result without damping controls and (b) shows the result with the damping control which is designed from the gain margin of 5 dB. In (a), the filter resonance is excited, and the primary current of the transformer and the output current have resonant distortions. It is noted that the experimental result in (a) shows the stability limit although the simulation result in Fig. 6 becomes unstable. This is because the loss of the multiple winding transformer and the multi-modular matrix converter behaves as a damping

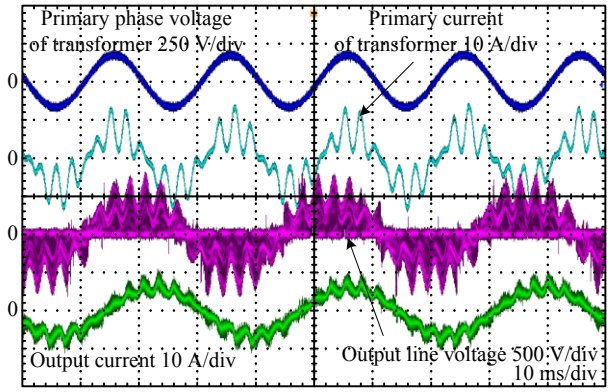

(a) Without damping controls which results in the primary current THD of 47.4% and the output current THD of 14.4%.

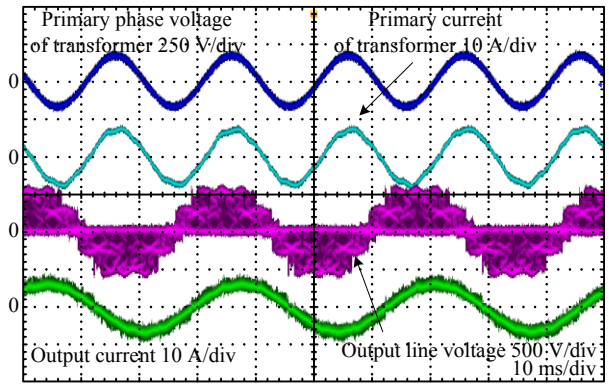

(b) With the proposed damping control which results in the primary current THD of 5.0% and the output current THD of 2.7%.

Figure 11. Input and output waveforms of the multi-modular matrix converter as illustrated in Fig. 1 in experiments.

resistor. The primary current THD (total harmonic distortion) of the transformer is 47.4% and the output current THD is 14.4% from Fig. 11 (a). In contrast, the filter resonance is suppressed and the system is stabilized by the damping control in Fig. 11 (b). As a result, the primary current THD of the transformer is 5.0% and the output current THD is 2.7%. Thus, the damping control mitigates the resonance distortions in the primary current by 89%. Furthermore, the output line voltage shows a 5-level waveform without the voltage fluctuation due to the filter resonance.

Fig. 12 shows the dq-axis output current in a transient response with the damping control which is designed from the gain margin of 5 dB. Note that this experiment fixes the output phase to 5 deg. in common with the simulation. The output current converges toward the reference because the damping control stabilizes the system. However, the d-axis current has an overshoot of 256% due to the damping control.

Fig. 13 shows the output current overshoot characteristics with respect to the designed gain margin. The experimental and simulation results of the output d-axis current overshoot increase together with the designed gain margin. This is because the damping control increases the gain in the lower

bandwidth as shown in Fig. 10 though the gain amplitude of the unit step is inversely proportional to the frequency. Therefore, the trade-off relationship between the stability and the transient response regarding the damping control is confirmed. The maximum error between the experimental and the simulation results is 11.2% and this error is due to the control and detection delays. In the future, the full consideration about this error will be reported.

VI. CONCLUSION

This paper discusses the stability analysis for a damping control combined with the output current control to suppress a LC filter resonance in a multi-modular matrix converter. Past works related to the design method of the conventional damping control applied to the input current control cannot be expanded into the proposed damping control. The analysis method uses Bode-diagrams based on the integrated block diagram of the whole system which is composed of the circuit and the control block diagram. Thus, the damping control can be designed easily since the effects of the resonant suppression and the output current response are yielded from the Bode-diagrams. From the simulation analyses, the designed damping control ensures the gain margin of 4.5 dB against a requirement specification of 5 dB, and a stable operation is achieved. From the experimental result, the multi-modular matrix converter with the designed damping parameters operates in stable condition, and the primary current of the transformer THD is suppressed by 89%. Therefore, the validity of the proposed stability analysis method is confirmed. In addition, the transient response characteristics of the output current control which is affected by the damping control are evaluated. As a result, the tradeoff relationship between the stability and the transient performance is illustrated clearly. In the future, the optimal design of the damping control will be considered.

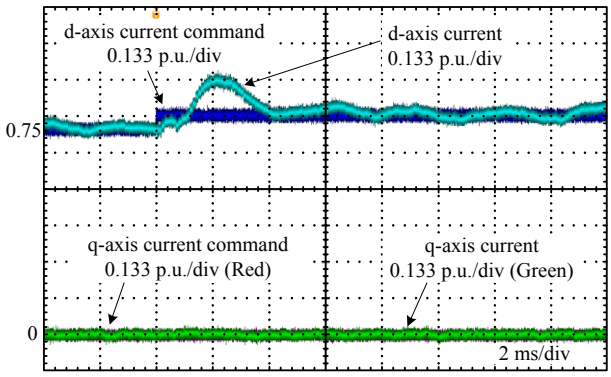

Figure 12. Output dq-axis current response with the damping control designed to obtain the gain margin of 5 dB. The output current converges toward the reference. However, the d-axis current overshoot of 256% is generated by the damping control.

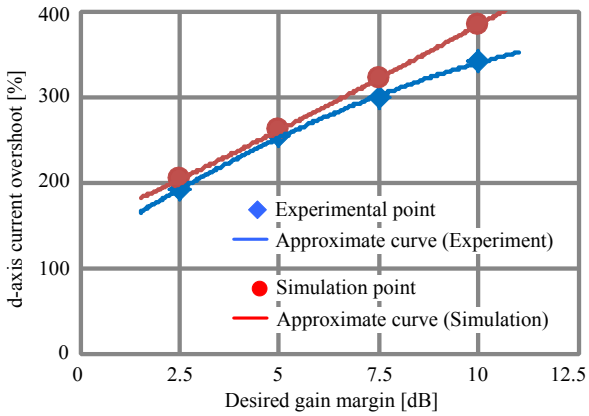

Figure 13. Output current overshoot characteristic with respect to the designed gain margin. This result shows the trade-off relation between the stability and the transient response regarding the damping control.

ACKNOWLEDGMENT

A part of this study was supported by Industrial Technology Grant Program in 2009 from New Energy and Industrial Technology Development Organization (NEDO) of Japan.

REFERENCES

[1] J. Kang, E. Yamamoto, M. Ikeda, E. Watanabe: "Medium-Voltage Matrix Converter Design Using Cascaded Single-Phase Power Cell Modules", IEEE Trans. Ind. Electron., Vol. 58, No. 11, pp. 5007-5013 (2011)

[2] E. Yamamoto, H. Hara, T. Uchino, M. Kawaji, T. J. Kume, J. K. Kang, H. P. Krug: "Development of MCs and its Applications in Industry", IEEE Industrial Electronics Magazine, Vol. 5, No. 1, pp. 4-12 (2011)

[3] J. Wang, B. Wu, D. Xu, N. R. Zargari: "Multimodular Matrix Converters With Sinusoidal Input and Output Waveforms", IEEE Trans. Ind. Electron., Vol. 59, No. 1, pp. 17-26 (2012)

[4] J. Wang, B. Wu, D. Xu, N. R. Zargari: "Indirect Space-Vector-Based Modulation Techniques for High-Power Multimodular Matrix Converters", IEEE Trans. Ind. Electron., Vol. 60, No. 8, pp. 3060-3071 (2013)

[5] H. Takahashi, J. Itoh: "Damping Control Combined to Output Stage for a Multi-Modular Matrix Converter", Proc. 28th IEEE APEC, (2013)

[6] T. Nunokawa, T. Takeshita: "Resonance Suppression Control in Complex Frame for Three-Phase to Three-Phase Matrix Converters", Proc. EPE2007, (2007)

[7] J. Haruna, J. Itoh: "Modeling Design for a Matrix Converter with a Generator as Input", Proc. 11th IEEE Workshop on Control and Modeling for Power Electronics, COM352 (2008)

[8] M. Rivera, C. Rojas, J. Rodriguez, P. W. Wheeler, B. Wu, J. Espinoza: "Predictive Current Control With Input Filter Resonance Mitigation for a Direct Matrix Converter", IEEE Trans. Power Electron., Vol. 26, No. 10, pp. 2794-2803 (2011)

[9] J. Haruna, J. Itoh: "Control Strategy for a Matrix Converter with a Generator and a Motor", Proc. 26th IEEE APEC, pp. 1782-1789 (2011)

[10] D. Casadei, G. Serra, A. Tani, L. Zarri: "Matrix Converter Modulation Strategies: Anew General Approach Based on Space-Vector Representation of the Switch State", IEEE Trans. Ind. Electron., Vol. 49, No. 2, pp. 370-381 (2002)

[11] Q.Guan, P. Yang, X. Wang, X.Zhang: "Stability Analysis for Matrix Converter with Constant Power Loads and LC Input Filter", Proc. 7th IPEMC 2012, pp. 900-904 (2012)

[12] J. Itoh, I. Sato, A. Odaka, H. Ohguchi, H. Kodachi, N. Eguchi: "A Novel Approach to Practical Matrix Converter Motor Drive System With Reverse Blocking IGBT", IEEE Trans. Power Electron., Vol. 20, No. 6, pp. 1356-1363 (2005)